Current Research in Microbial Sciences 3 (2022) 100109

Contents lists available at ScienceDirect

Current Research in Microbial Sciences

journal homepage: www.sciencedirect.com/journal/current-research-in-microbial-sciences

An Arabidopsis nonhost resistance gene, *IMPORTIN ALPHA 2* provides immunity against rice sheath blight pathogen, *Rhizoctonia solani*

Daraksha Parween, Binod Bihari Sahu *

Laboratory of Molecular Genetics and Plant Immunity, Department of Life Science, National Institute of Technology Rourkela, Odisha 769008 India

ARTICLE INFO

Keywords:
IMPA2
Infection cushion
Nonhost resistance
Necrotroph
Rhizoctonia solani
Sheath blight

ABSTRACT

There is neither resistant rice cultivar nor any control measure against *Rhizoctonia solani* AG-1 IA (*RS*), causal of sheath blight and a major threat to global rice production. Rice is a host and Arabidopsis is a nonhost with underlying nonhost resistance (NHR) gene which is largely untested. Using approaches of forward genetics and tools, cytology, and molecular biology, we identified homozygous mutants in Arabidopsis, mapped the NHR gene, and functionally characterized it in response to *RS*. *Rss1* was mapped on Ch 4 between *JAERI18* and *Ch4_9.18* (844.6 Kb) and identified *IMPORTIN ALPHA 2* as the candidate *RSS1* gene. We found that breach of immunity in *rss1* by *RS* activates defense responses whereas photosynthetic pigment biosynthesis and developmental processes are negatively regulated. In addition, a gradual decrease in *PR1* by 3 dpi revealed that *RSS1* positively regulated early SA-mediated resistance. Whereas increased expression of *PDF1.2* by 3 dpi supported switching to necrotrophy, SA-mediated defense in Col-0 leading to immune response. Enhanced expression of *ATG8a* in rss1 supported autophagic cell death. *IMPA2, IMPA1*, and *RAN1* function together to provide NHR against *RS*. These findings demonstrate that *IMPA2* provides NHR against *RS* in Col-0 that evoke SA-mediated early immunity with boulevard for potential biotechnological application.

1. Introduction

A constant increase in the world's population to 9.15 billion by 2050 put immense pressure to increase the agricultural food security demand by 60–100% globally (Alexandratos and Bruinsma, 2012). It is a major quagmire to achieve and fulfill the global food sovereignty with demand wherein rice is the common and most important staple food worldwide. Sheath blight in rice is the second most devastating necrotrophic fungal disease by the causative agent, *Rhizoctonia solani* Kuhn AG1-IA (*RS*) with varied host range, a severe necrotrophic basidiomycete fungus contributing to a yield loss of around 50% worldwide (Mishra et al., 2020; Molla et al., 2020). The early infection process of *RS* includes hyphal colonization with atypical "infection cushions" and swollen hyphal tips and necrotic lesion formation for which there has neither been a tolerant variety of rice nor any control measure (Basu et al., 2016). Host-specific toxins effector molecules, *AGLIP1, RsIA_NP8*, glycosyltransferase, cytochrome C oxidase, and peptidase inhibitor I9 domain produced by *RS* target the defense signaling pathways leading to successful colonization and enhancing rice sheath blight (Li et al., 2021).

To protect against pathogenic invaders, plants perceive the danger signal such as Pathogen/Danger-associated molecular patterns by using the cell surface pattern recognition receptors leading to activation of pattern-triggered immunity. However, pathogens secrete an arsenal of effectors to subdue the potential immunity generated against them which further leads to activation of cognate *R*-genes in plants via NLR-mediated immunity which is termed effector-triggered immunity (Ngou et al., 2021). Although the gene-for-gene model with specific *R*-gene mediated immunity in plants persists, nonhost resistance (NHR) prevents successful colonization against certain pathogens. NHR are multi-gene trait exhibiting defense in all plant species against all races of pathogens and are broad-spectrum and more durable which can be a long-hoped goal of plant pathologists for successfully transferring the NHR gene(s) to the susceptible host (Gill et al., 2015; Mysore and Ryu, 2004; Stein et al., 2006). NHR comprises a two-layered defense mechanism i.e., pre-and post-invasive resistance (Lipka et al., 2005). *NON-HOST 1* (*NHO1*) is the first identified NHR gene reported to provide immunity against species of bacteria, *Pseudomonas fluorescens, P. syringae* pv. *tabaci* and *P. syringae* pv. *phaseolicola*, as well as necrotrophic

Abbreviation: Alpha, α; Beta, β; Day post-inoculation, dpi; Hour of post-inoculation, hpi; *Rhizoctonia solani*, *RS*; Next-generation sequencing, NGS; Nonhost resistance, NHR; IMPORTIN ALPHA 1, IMPA1; IMPORTIN ALPHA 2, IMPA2; Ras-related nuclear protein, RAN1; *R. solani susceptible 1*, *rss1*.

* Corresponding author.
E-mail address: sahub@nitrkl.ac.in (B.B. Sahu).

https://doi.org/10.1016/j.crmicr.2022.100109
Received 24 December 2021; Received in revised form 31 January 2022; Accepted 6 February 2022
Available online 8 February 2022

fungus *Botrytis cinerea* (Kang et al., 2003; Lu et al., 2001). Forward genetics screening revealed the well-known *PENETRATION* genes of Arabidopsis i.e., *PENETRATION1 (PEN1), PEN2, PEN3,* and *PEN4,* involved during pre-invasive resistance, essential in providing NHR against barley powdery mildew pathogens *Blumeria graminis* and *Erysiphe pisi* (Micali et al., 2008).

Notably, several genes have shown NHR to different necrotrophic fungi. *PEN2* conferred penetration resistance against hemibiotrophic fungus *Magnaporthe oryzae* (Maeda et al., 2009) and necrotrophic fungus *RS* (Parween et al., 2021), the causal agents of rice blast and rice sheath blight respectively. The *PEN4* (phytochelatin synthase (*PCS1*), plays its role in heavy metal stress tolerance, also provide pre-invasive NHR against *B. graminis* and *M. oryzae* (Hematy et al., 2020; Yamaura et al., 2020). *PAD4* and *SAG101* have been reported to provide broad-spectrum NHR in Arabidopsis against *B. graminis* stimulating SA production and antimicrobial molecules (Dongus et al., 2020; Lapin et al., 2020; Lipka et al., 2005). Arabidopsis *PSS1* (*PHYTOPHTHORA SOJAE SUSCEPTIBLE 1*) and *PSS30* encoding a glycine-rich protein (GRP) and *FOLATE TRANSPORTER1* respectively are required for pre-and post-penetration resistance against *Phytophthora sojae* and *Fusarium virguliforme* in field conditions (Kambakam et al., 2021; Sumit et al., 2012; Wang et al., 2018). Mutation in barley *mlo5* (*MILDEW RESISTANCE LOCUS O*), Arabidopsis *ABCG34I* (ABC transporter), different signaling pathways like *ein2* and *ein3* (ET), *pad2*, *pad3, eds4, eds8* (SA), *iop1, coi1* and *jar1* (JA) lead to a breach of immunity against the necrotrophic fungus species (Alonso et al., 2003; Denby et al., 2004; Ferrari et al., 2003; Khare et al., 2017; Kiraly, 2002; Solano, 2002; Thomma et al., 1998). Although the molecular mechanism of NHR is not very well understood, the practical application of NHR using transgenic approaches has been tested in field conditions producing disease-resistant crops (Fonseca and Mysore, 2019). QTLs reported against *RS* may be introgressed to generate resistant rice germplasm which however does not work in field conditions as fungal pathogens develop resistance in due course of time (Yellareddygari et al., 2014).

Since rice is susceptible to *RS* and Arabidopsis is a nonhost with the active defense during early infection, it is possible to identify the underlying NHR gene. To address this, we generated rss1 in Col-0 background with compromise in early immunity against *RS*. Here, we mapped *RSS1* on the southern arm of Chromosome 4 between *JAERI18* and *Ch4_9.18* and identified it which encodes an *IMPORTIN ALPHA 2 (IMPA2)*. We observed that *rss1* showed severe HR and cell death upon *RS* infection which affected in negative biogenesis of the photosynthetic pigments. Furthermore, *IMPA2* governs SA-mediated early immunity, and *rss1* leads to *RS*-induced autophagic cell death. The result suggests that *IMPA2* activates the HR and does not allow the establishment of infection structure in Arabidopsis thereby confers early immunity to *RS*.

2. Materials and methods

2.1. Growing conditions and accessions

Arabidopsis seeds of wild type, Col-0 (N1093) and T-DNA insertion lines *impa-2* (SALK_017914 and SALK_099707), *impa-1* (SALK_082616), *ran1–1* (SALK_138,680), and *ABC1* (SALK_045739) were obtained from NASC, Europe. The seeds were sown on flats containing agro peat and vermiculite (3:1), covered with plastic wrap, and stratified for 1 day at 4 °C before transferring to plant growth chamber. Seedlings of rice and Arabidopsis accessions were grown as described previously (Parween et al., 2021).

2.2. RS culture condition and inoculation assay

RS AG-1 IA isolate was cultured regularly on freshly prepared potato dextrose agar (PDA) medium and kept at 28 °C for ~14 days in dark conditions. The sclerotia development was visible at 7-day old culture on Petri dishes. Spectinomycin (100 μg/ml) was used to avoid any bacterial contaminations.

To study the infection pattern and development of *RS* mycelia in rice and Arabidopsis, detached leaf and in planta infection assay was performed as mentioned earlier (Parween et al., 2021). Briefly, the detached leaves of the 4th leaf stage of rice and 24− old Arabidopsis seedlings were infected with equi-sized sclerotia (2–4 mm in diameter) from the 10-day old *RS* grown PDA plates. The infected leaves were placed in a Petri plate on sterile water moistened filter paper and covered to maintain high humidity until used for the study.

2.3. Generation of Arabidopsis mutants and mapping population

Around 25,000 Col-0 seeds (M0) were mutagenized by treating with various concentrations of ethyl methane sulphonate (EMS at 0.3%) for 12 h following Qu and Qin (2014). M_1 seeds (mutated seeds from above) were sowed onto soil and grown by maintaining the growth conditions as above. The mutated seedlings showed phenotypes like stunted growth and dis-coloration pattern of leaves which might be resulting from a mutation in the gene(s) across the genome. Further, M_1 plants were grown to get M_2 seeds for the test of homozygosity of susceptible phenotype by infecting the detached leaves with *RS* that causes rice sheath blight.

To generate an F_2 population to map the mutated gene, we chose the resistant wildtype ecotype of Arabidopsis (Ler-0) and crossed it with homozygous susceptible M_3 plants. F_1 seedlings were confirmed using SSLP markers *(NGA106* and *LUGSSLP671*). F_2 seeds harvested from true F_1 seedlings, and the population thus generated was used for disease scoring and mapping the gene.

2.4. Staining and microscopy analysis

Trypan blue, DAB, and aniline blue staining were performed as described earlier by Park et al. (2009). Stained leaves were observed under brightfield, and fluorescence microscope images were recorded for screening. Determination of H_2O_2 accumulation (ROS) in Arabidopsis leaves was also determined using 2′, 7′-dichlorodihydrofluorescein diacetate (H_2DCFDA) - mediated fluorescence, as previously described by Zeng et al. (2015). Determination of superoxide accumulation was done using nitroblue tetrazolium (NBT) where formazan (dark blue stain) is formed upon reaction with superoxide (Fryer et al., 2002). Infected leave samples were also stained with Calcofluor White stain (18,909 Merck), which binds to fungal chitin and check the progression of *RS* hyphae . Infected leave samples were placed on a clean glass slide and a drop of Calcofluor White stain followed by a drop of 10% KOH solution was added. It was allowed to incubate for 1–2 min and was examined under a confocal microscope (Leica TCS SP8).

2.5. Live cell photosynthetic pigments imaging and chlorophyll estimation

Live cell imaging of the chloroplast autofluorescence was measured under a Laser scanning live-cell imaging microscope (Leica, STELLARIS 5) with an excitation of 633 nm and emission of 647–721 nm (Irieda and Takano, 2021). Chlorophyll (chl) estimation in the infected leaves was performed as elaborated in Parween et al. (2021).

2.6. Electrolyte leakage assay

Electrolyte leakage assay was performed as previously described by Jamra et al. (2021). Briefly, fifteen leaves from 24th-day-old seedlings were challenged with *RS*. Freshly harvested infected detached leaves discs (15 numbers) that were submerged in 10 mL of sterile water and shaken gently and the membrane leakage (electrolytes (ions) (μΩ−1) leaked (IL initial) was measured by a conductivity meter from the . The samples were then subjected to boiling in a water bath for 15 min and final conductance was measured (IL Final). Percentage (%) of ion leakage was calculated as

$$\% \text{ of IL} = \left(\text{IL}\frac{\text{initial}}{\text{final}}\right) \times 100$$

2.7. Mapping of NHR gene

Genomic DNA was isolated from the screened individual seedlings of the F_2 population using the CTAB method (Lukowitz et al., 2000). An equal amount of genomic DNA was pooled from F_2 lines to make separate bulks of S_1 (moderately susceptible), S_2 (highly susceptible), and R (resistant) for bulk segregation analysis (BSA). PCR was done using individual bulked lines to map the possible region of the candidate gene responsible for disease phenotype. We used simple sequence length polymorphism (SSLP), Cleaved amplified polymorphic sequences (CAPS), and sequence-based polymorphic (SBP) markers that are evenly distributed throughout the genome of Arabidopsis. Additional SBP markers were designed as described earlier (Sahu et al., 2012). Markers used for PCR analysis are mentioned in Table S5. Bulked S_2 DNA (100 ng) was then sent for Illumina sequencing (3i Molecular solutions, Bangalore, India). FASTQ data obtained from the next-generation sequencing (NGS) were converted to BCF format (.bcf) using SIMPLE pipeline. The rss1.bcf file was uploaded to the next-generation mapping (NGM) portal (http://bar.utoronto.ca/NGM) to visualize, give SNP calls and analyze the data (Austin et al., 2011).

2.8. RNA extraction and RT-qPCR analysis

Total RNA was extracted from the mock and infected leaf samples of rice and Arabidopsis accessions at different inoculation times using the TRIzol® reagent (Invitrogen). Purity and concentration of RNAs were then quantified using Nanodrop (Bio spectrophotometer, Eppendorf) and 1% agarose gel electrophoresis. Further, DNase I (Novagen, Millipore) treatment was performed to get rid of genomic DNA which was confirmed by performing a -RT-qPCR reaction using *AtACTIN2* primer pair. RNA samples were then used to synthesize cDNAs at 25 °C for 10 min, 42°C for 60 min, and followed by 75 °C for 15 min using a Thermo Scientific cDNA synthesis kit. The expression level of SA- (*AtPR1, AtICS1*), JA (*AtPDF1.2a*), leaf senescence (*AtNHL10*), autophagy (*AtATG8*), and *AtIMPA2* marker genes were estimated which was normalized to the expression of *AtACTIN2* as an internal control. The expression level in rice was analyzed using gene-specific primers of *OsPR1, OsPDF1A* and normalized with *OsActin*. Primers used in this study are mentioned in Table S6. qPCR was performed using SYBR Green Master Mix (Bio-Rad) in a Real-Time system (Bio-Rad) and relative expression levels were calculated using the $2^{-\Delta\Delta Ct}$ method (Pfaffl, 2001).

2.9. Statistical and in silico analysis

For the detached leaf infection assay, a minimum of three leaves per plant and 3 seedlings of each Arabidopsis accessions and rice (Swarna) were used. Each experiment was conducted with three biological replicates and similar results were obtained in three independent experiments. All the graphs represent mean (± SD) where statistical significance analysis was performed using Student's *t*-test for two groups and two-way ANOVA for multiple comparisons using GraphPad Prism 7. Relative intensities of trypan blue, DAB, H_2DCFDA were calculated using GIMP 2.10.10 (Scalschi et al., 2015). ImageJ: IJ 1.46r (Schneider et al., 2012) was used to measure the necrotic lesions for disease severity. Domain prediction using the deduced protein sequence was performed at the SMART online tool (Letunic et al., 2020).

3. Results

3.1. Identification of RS-susceptible Arabidopsis mutant with compromise in immunity

Arabidopsis (Col-0) is a nonhost to *RS* (Parween et al., 2021). The presence of NHR genes providing immunity against *RS* in Col-0 is preclusive to the disease occurrence. To find the putative resistance genes, seeds of Col-0 were mutagenized by 0.3% (w/v) EMS. The M_1 progeny clearly showed dis-coloration of leaflets (Fig. S1A) and stunted growth (Fig. S1B). M_1 seeds were harvested individually and stored at 4 °C until further use. We screened the detached leaves from the M_2 seedlings for susceptible responses by infecting them with *RS* sclerotia. Further, the homozygous mutants were isolated in M_3 generation and named the most susceptible plant as *Rhizoctonia solani susceptible* 1 (*rss1*). The pathogenicity of *RS* at 48-h post-inoculation (hpi) was also validated in the *rss1* plants through trypan blue (Fig. S1C), DAB (Fig. S1D), and aniline blue (Fig. S1E) staining.

The pathogenicity of *RS* in *rss1* with a susceptible response as early as 30 hpi was depicted by infection cushion was confirmed by trypan blue (Fig. 1A) and accumulation of H_2O_2 as marked by brown precipitate from DAB staining (Fig. 1B). Trypan blue stained *rss1* leaves infected by sclerotia of *RS* showed heavy mycelia with branched atypical infection cushions and maximum colonization as compared to Col-0 which showed perpendicular runner hyphae. DAB staining showed a significantly higher accumulation of H_2O_2 in *rss1* at infection sites as compared to Col-0. Graphical representation of trypan blue and DAB intensities showed significantly high stain uptake in *rss1* as compared to Col-0 (Fig. 1C).

It was therefore of interest to compute the cell death from detached leaves of Col-0 and *rss1* challenged with *RS* at 30 hpi through ion leakage assay. The *RS*-treated leaves of *rss1* showed enhanced cell death as compared to Col-0 where the ion leakage values ($\mu\Omega^{-1}$) obtained were normalized to the respective water control (Fig. 1D). The severity of *RS* on *rss1* was also validated through *in planta* infection assay using similar sizes of sclerotia and disease phenotypes were observed at 0, 3, and 6 dpi (Fig. 1E). The *rss1* exhibited compromised immunity to the nonhost pathogen, *RS*, that showed a higher disease lesion area as compared to Col-0 with increasing time points.

3.2. Molecular mapping of RSS1 by bulked segregant analysis and its identification via NGM analysis

To identify the putative mutated gene responsible for *RS* pathogenicity in *rss1*, we followed the bulked segregant analysis, and *rss1* was crossed with Ler-0 (resistant ecotype of Arabidopsis). The true F_1 seedlings produced from the above outcross were confirmed genotypically by using *NGA106* (Fig. S2A) and *LUGSSLP671* (Fig. S2B). F_2 population thus generated was screened further with *RS*, followed by trypan blue staining, and their infection phenotypes were observed under a bright-field microscope. Subsequent bulking of F_2 progeny was done based on the disease phenotype screening against *RS*. They are denoted as resistant (R), mycelia growing over leaf surface with the initiation of infection cushions (S1) and leaves with infection cushions and profuse mycelial branching (S2), representing low, medium, and highly susceptible phenotype (Fig. S2C). Thirteen out of 54 F_2 seedlings were found to be super-susceptible (S2). Screened infected leaves of the F_2 population showed a 3:1 Mendelian inheritance ratio, indicating a single recessive gene, *RSS1* controlling the NHR in Col-0 (Table S1). We pooled the genomic DNA from the thirteen susceptible seedlings and performed the bulked segregant analysis using evenly placed molecular markers (SSLP, CAPS, and SBP) across all the 5 Chromosomes (Figs. S4–S8). It was found that the *RSS1* putatively maps to the lower arm of Chromosome 4 flanked by *JAERI18* and *TGSSLP2*. Fine mapping of the F_2 population confines the map location of *RSS1* to 844.6 Kb that is localized between *JAERI18* and *CH4_9.18* (Fig. 2A; Table S2).

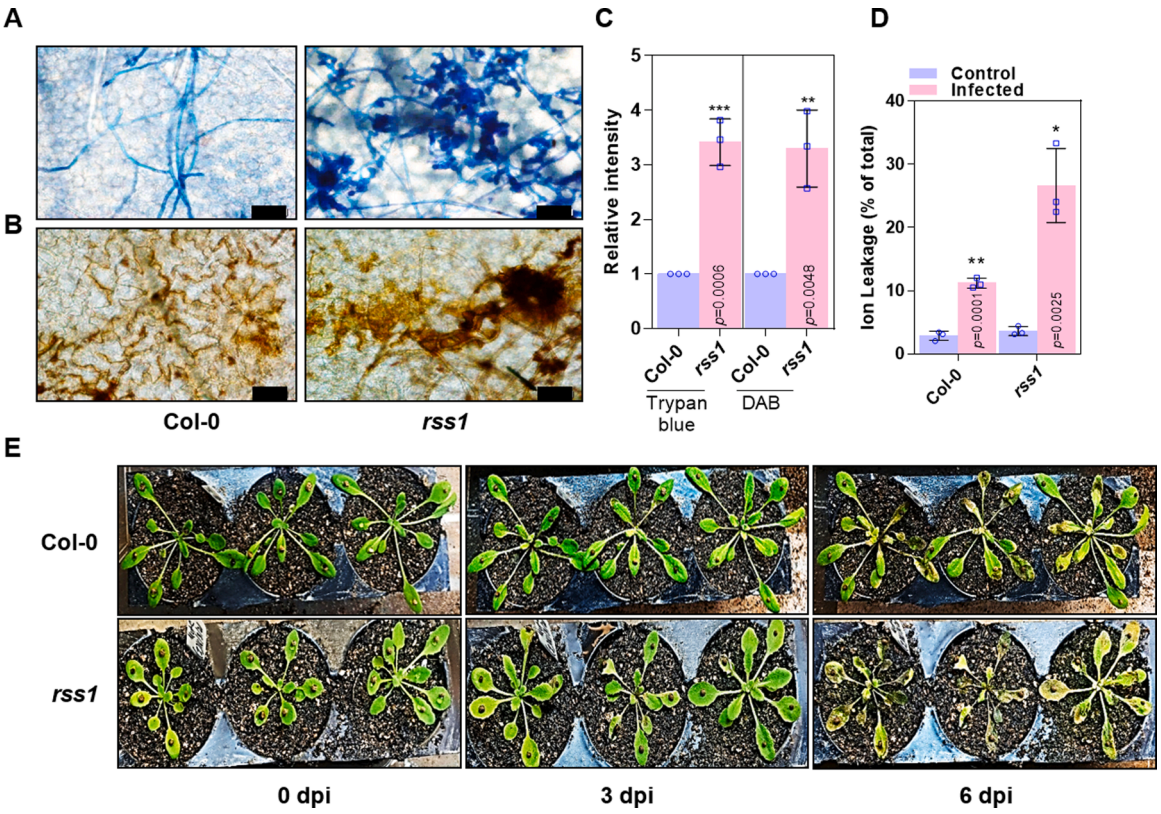

Fig. 1. EMS-induced homozygous mutant of Arabidopsis is infected by multinucleate basidiomycete *RS*. (A) Detached leaf infection assay of wild type Col-0 and *rss1* at 30 hpi using trypan blue (upper panel) and DAB staining (lower panel). Bar=50 μm. (B) The intensities of trypan blue- and DAB-stained fungal hyphae in *rss1* were quantified using GIMP and normalized with the intensity of Col-0. The bar represents the mean (± SD) from at least three biological replicates (n = 3). Unpaired Student's *t*-test was performed for significance analysis. (C) Ion leakage assay was performed using *RS* infected leaf discs (6 mm Dia) of Col-0 and *rss1* and it was normalized with the data (μΩ−1) of leaf disk treated with water that acted as the control. The bar represents the mean (± SD) from at least three biological replicates (n = 3). (D) Necrotrophic lesions as disease symptoms in 4-week-old rosette leaves in seedlings of Col-0 and rss1 challenged with ~3–4 mm sclerotia of *RS* in planta and were imaged at 0, 3rd, and 6th-day post-inoculation (dpi).

The pooled genomic DNA was sent for -NGS and data obtained were run via SIMPLE pipeline upon trimming of the adaptors and aligned to TAIR-10 reference genome. The *rss1.bcf.ngm* file thus generated was used to visualize the positional mapping of the candidate gene responsible for *RS* susceptibility at the online tool called NGM (Next-generation EMS mutation mapping). Genome-wide filtered SNPs were plotted based on their abundance over each chromosome, and we found that the southern arm of Chromosome 4 showed non-recombinant (Fig. 2B). The NGM analysis was based upon discordant chastity (Ch_D) value of 1 which comprehends the expected homozygous mutated allele as compared to the reference genome. Also, the chastity threads were generated by applying a higher *k*-value (*k*-means clustering, $k = 7$) which increases the homozygous to heterozygous ratio, and smaller kernel size (kernel density=0.25) to refine and validate the candidate SNPs responsible for the causal phenotype (Fig. 2B, C). From the NGM mapping tool, we found two SNPs leading to nonsynonymous mutations (Table S3) at the mapped region on Chromosome 4. We screened all the respective T-DNA insertion SALK line mutants (Table S4), compared them with the Col-0 to find out the casual mutated gene responsible for *RS* susceptibility. The *SALK_017914* was found with a similar infection cushion in leaves as the *rss1* confirms that *At4g16143* is the candidate *RSS1* gene responsible for immunity against *RS* (Fig. 2D).

Moreover, *SALK_099707* (an additional homozygous T-DNA insertion line in the 7th exon of *At4g16143*) also showed infection hyphae trying to enter through stomata (Fig. 2D), and a greater number of atypical infection cushion formation than the other T-DNA insertion lines (data not shown). The SNP in *AT4G16143* (*IMPA2*) in *rss1* was identified as a G→A substitution (9,136,942 on Chromosome 4) in the first exon that results in the replacement of the Pro-by Ser-in the 65th amino acid which was also confirmed by sequencing (Fig. 2E and F, marked by an asterisk). The $^{P}65_{S}$ of impaired IMPA2 falls in the autoregulatory region in the IBB domain that binds to importin beta to make ternary complexes and it has 8 armadilo repeats (Fig. 2F). We labeled the two T-DNA insertion lines *SALK_099707* as *rss1–1* and *SALK_017914* as *rss1–2*. The molecular mapping, NGM analysis of the NGS data, and early hour infection assays suggest that a non-synonymous mutation of *AT4G16143* (*IMPA2*) in *rss1* compromised penetration resistance in Col-0 against *RS*. We aligned all 9 paralog protein sequences of Arabidopsis. IMPA2 had 85.63% similarity with IMPA1 (*At3g06720*) and 6 rice orthologs where IMPA2 has shown 80.50% similarity with importin subunit alpha-1a-like (*Os01g14950*) and 79.43% with importin subunit alpha-1b (*Os05g06350.1*) (Table S7). Further, the mutated proline at 65th position in *rss1* was found to be conserved in IMPA2 and we speculated the similar functionality of the paralog in providing defense against *RS*.

3.3. Sheath blight resistance in Arabidopsis is conferred by the IMPA2

We evaluated the disease severity during nonhost-*RS* (Col-0-*RS*) interaction based on macroscopic symptoms and lesion sizes as compared to that of host-*RS* (Rice- *RS*) (Fig. 3A–C). Gradual increases in chlorotic and necrotic lesions were observed in *RS* challenged rice (Swarna) leaves at 1, 2, and 3 dpi (Fig. 3A). Col-0 was resistant with much lesser or no signs of visual necrotic lesion up to 3 dpi at the infection site whereas leaves of *rss1, rss1–1,* and *rss1–2* showed similar necrotic lesions (banded krait) like rice (Fig. 3B). The percentage of

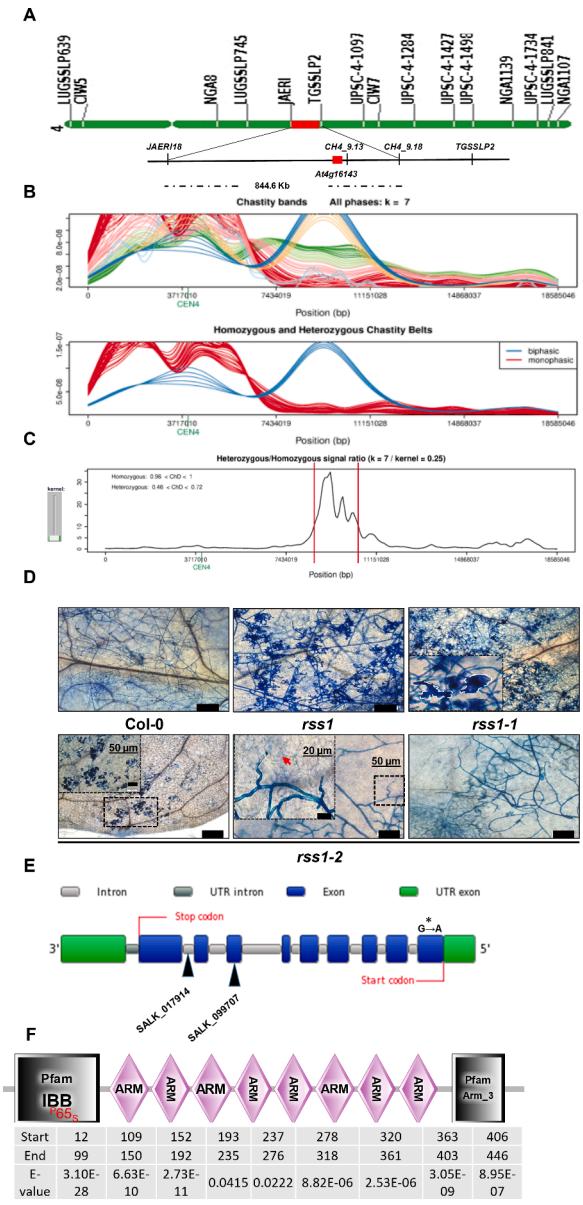

Start	12	109	152	193	237	278	320	363	406
End	99	150	192	235	276	318	361	403	446
E-value	3.10E-28	6.63E-10	2.73E-11	0.0415	0.0222	8.82E-06	2.53E-06	3.05E-09	8.95E-07

Fig. 2. Mapping and identification of putative *RSS1* on Chromosome 4 via NGM analysis. (A) Mapping of *RSS1* onto Chromosome 4 between *JAERI18* and *CH4_9.18*. (B) NGM view of the aligned NGS data which depicts the homozygosity chastity belts across the Chromosome 4 by keeping the CD value to be 1. (C) The window highlights the region onto the Chromosome 4 of the homozygous belt to derive the nonsynonymous SNPs (Table S3). (D) Screening of two T-DNA insertion lines (SALK_099707 as *rss1–1* and SALK_017914 as *rss1–2*) of the putative *RSS1* independently for disease phenotype as above with a comparison to the identified homozygous rss1. Microscopic observations of the trypan blue stained leaves at 2 dpi showed the development of similar atypical infection cushions in T-DNA insertion lines to that of *rss1*. Inset figures depicts the zoom-in pictures. Stained leaves were observed under a bright-field microscope. Bar=100 µm. (E) The schematic representation of *RSS1* (*At4g16143*; encoding *IMPORTIN ALPHA 2*) identified with a substitution of guanine (G) with adenine (A) leading to $^{P}65_{S}$. The places of two T-DNA insertion Arabidopsis accessions with different target sites in *IMPA2* gene (marked by black shaded triangles) and site of EMS generated point mutation (marked by a black star) in the first exon. (F) Schematic diagram of the domains predicted online. The nonsynonymous mutation in the IBB domain at the 65th position is depicted. The underneath amino acid span length corresponds to specific domains with predicted E-value are tabulated.

disease severity was calculated based on the disease spread from the observed visible browning lesions on leaves with a necrotic lesion at 3 dpi in *rss1* was highest (Fig. 3C). To assess *RS*-induced macroscopic lesion resulting from the HR process with a gradual increase in time, we studied the infection phenotypes by microscopy on the leaves of Col-0, *rss1 rss1–1,* and *rss1–2* using trypan blue in the whole leaf (Fig. 3D). Among all, *rss1* showed an enhanced mycelial mass of *RS* and maximum lateral branching marked by irregular-shaped dark blue regions on the epidermal cell surface, shown by infection on the whole leaf (left panel) and microscopic image (right panel) at 1 dpi. At 2 dpi and 3 dpi, *RS* continued to proliferate in *rss1* with profuse mycelial branching, extensive colonization, and the formation of infection cushions (Fig. 3D). *rss1–1* and *rss1–2* indistinctly showed similar infection severity like *rss1* whereas Col-0 only showed entangled, right-angled branching of mycelia entrenched on the leaf surface with increasing time points. The image represents one of the representative experiments from each ecotype, with similar results. Based on these microscopic images, the relative intensity of trypan blue was quantified, showing higher intensity in *rss1* than *rss1–1* and *rss1–2* which was normalized with the intensity of Col-0 (Fig. 3E).

To monitor the induced cell death after infection, the percentage of released electrolytes was measured. The increase in cell death count was significantly higher in *rss1* than *rss1–1* and *rss1–2* as compared to Col-0. *rss1* showed an increase of ~70% ion leakage at 3 dpi (Fig. 3F). Our observation indicates that *RS* infection in *rss1* was found to be increasing in a spatiotemporal manner. To further visualize the infection in *rss1*, we checked the micrograph with *z*-stack imaging in a confocal microscope (staining by calcofluor White) and found the surface to in-depth spread and colonization of the entangled mycelia at 3 dpi (Figs. 3G, S3). The infection cushion development was barely visible in Col-0, whereas there were enormous infection cushions that are evident in the *rss1* and *rss1–1*. This suggests that the significant breach in immunity is due to point mutation in the *IMPA2* and its knockout in Arabidopsis respectively.

3.4. *Impaired IMPA2 and its knockouts show accumulation of RS-induced reactive oxygen species and callose deposition*

Production of hydrogen reactive oxygen species and accumulation of callose at the site of successful infection in the plant are the early defense responses to biotic stress (Bolwell and Daudi, 2009; Ellinger and Voigt, 2014). We investigated the pattern of H_2O_2 accumulation from Arabidopsis in *rss1* at 1 dpi, 2 dpi, and 3 dpi. Microscopy images depict higher H_2O_2 accumulation in *rss1* than the Col-0 with increasing time points (Fig. 4A). Furthermore, the T-DNA insertion mutants *rss1–1* and *rss1–2* also showed similar phenotypes like *rss1* leaves. The relative intensity of DAB was also quantified digitally which showed a significant difference among Col-0 and respective *rss* mutants (Fig. 4B). This result was further substantiated by using H_2DCFDA in live infected tissues, which upon reaction with ROS produces a highly fluorescent product i.e., 2′, 7′-dichlorofluorescein. *rss1* and T-DNA insertion lines showed maximum localization and accumulation of ROS which were indistinctly accumulated in the Col-0 cells at 30 hpi (Fig. 4C). Relative fluorescence intensity of H_2DCFDA showed a significant difference among Col-0 and mutants (Fig. 4D). A higher accumulation of superoxide ions, $O_2^{\bullet-}$, another important component of ROS, was observed in the infected leaves of *rss1, rss1–1,* and *rss1–2* at 30 hpi using NBT stain (Fig. 4E). This correlation amongst the microscopic symptoms augmented levels of H_2O_2 and $O_2^{\bullet-}$ accumulation in *rss1* and SALK mutants suggests that *RSS1* could be involved in negatively regulating hypersensitive response and compromised penetration of *RS*.

Callose, a (1,3)-β-glucan cell wall polymer, is a common constituent of papillae formation which marks the entry sites of a pathogen (Aist, 1976). Papillae act as a physical barrier that restrict pathogen colonization (Stone and Clarke, 1992). An intensified noticeable callose deposition was observed at the fungal infection sites of inoculated

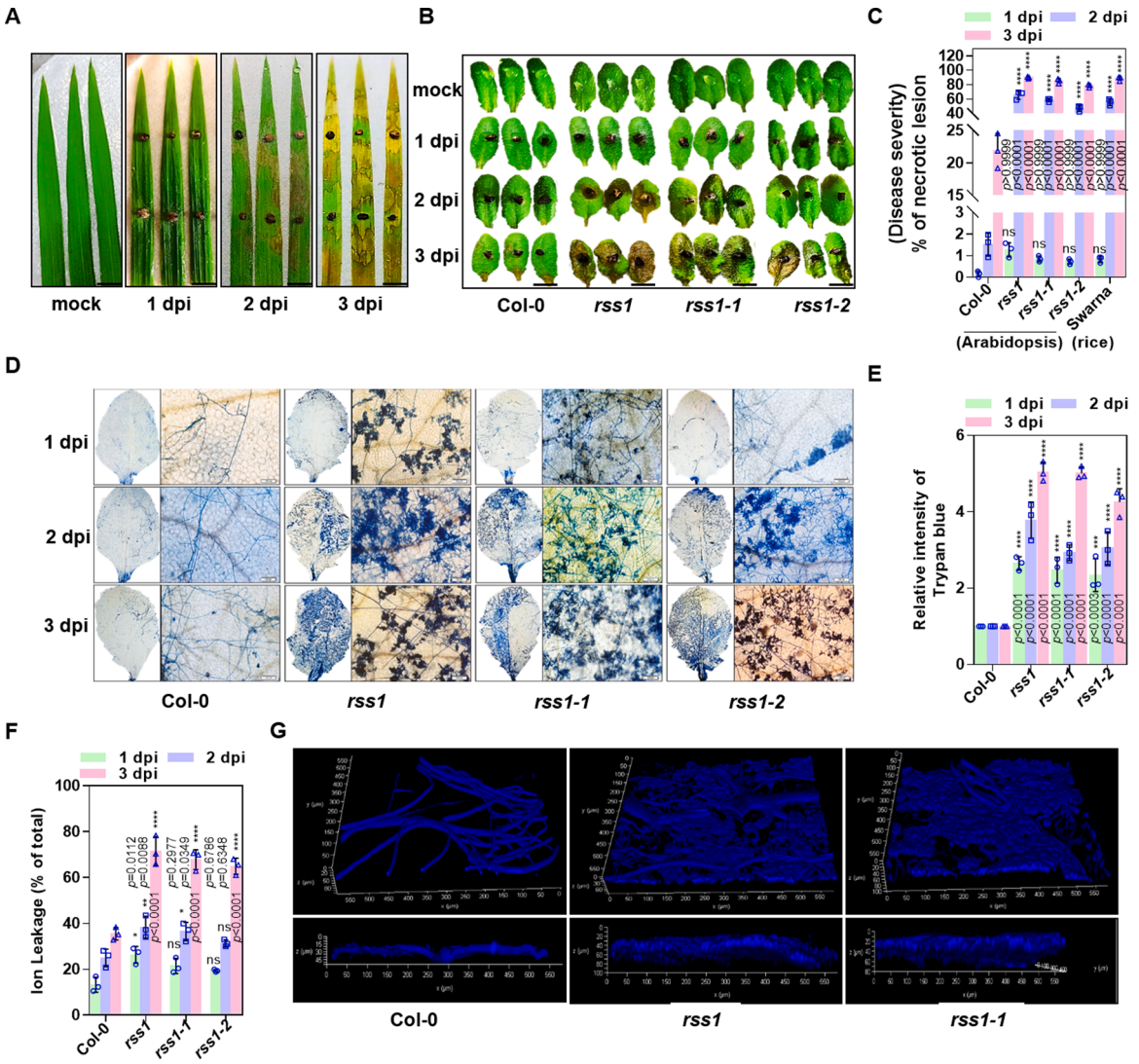

Fig. 3. *RS* infection in Arabidopsis contributed to hypersensitive cell death response and penetrated to colonize in mutants. (A) Lesion development on rice (Swarna) and (B) Arabidopsis (Col-0) and *rss1, rss1–1,* and *rss1–2* leaves were photographed after inoculation with *RS* sclerotia at 0, 1, 2, and 3 dpi. (C) The graph represents the percentage of lesion areas, measured at different time points using ImageJ. The bar represents the mean (± SD) from three biological replicates (n = 3). Similar results were obtained in three independent experiments. (D) *RS* infected Arabidopsis leaves from at 1, 2, and 3 dpi were stained with trypan blue. Dark, blue-stained infection cushions were detected in *rss1, rss1–1, rss1–2* while only runner hyphae were observed in Col-0 leaf surface (right panel; photomicrographs). Mutants showed more attempted penetration sites than Col-0. Bar= 5 mm (A, B, D-Left panel)100 μm. (E) Based on the microscopic images of (D), the intensity of trypan blue-stained fungal hyphae in *rss1, rss1–1*, and *rss1–2* was quantified and normalized with the intensity of Col-0 obtained from GIMP. The bar represents the mean (± SD) from three biological replicates (n = 3). Similar results were obtained in three independent experiments. (F) Ion leakage was measured in *rss1, rss1–1,* and *rss1–2* and compared with Col-0, after inoculation with *RS* at 1,2, and 3 dpi. The graph represents mean (± SD) which were calculated from fifteen leaf disks per treatment, with three replicates within an experiment. Similar results were obtained in three independent experiments. (G) Z-stack images of infected leaves of Col-0, *rss1*, and *rss1–1* at 2 dpi were analyzed to study and validate the hyphal colonization of surface mycelia. Infected mutant leaves showed profuse hyphal branching with infection cushions (upper panel). The 3D image showed maximum development of fungal colonization with varying depth in the accessions studied i.e., ~100 μm in *rss1*, ~80 μm in *rss1–1*, whereas it was ~45 μm in Col-0 (lower panel).

mutant leaves as an attempted entry by *RS* when assessed with the WT at 3 dpi (Fig. 4F). An increase in callose deposition was observed in *rss1* and *rss1–1* leaves upon infection which however is inhibited in WT, which may be preventing further entry of the pathogen. This reveals that the mutant can still recognize the infection and react competently. Relative expression of *GSL5*, a pathogen-induced callose biosynthesis marker (Enns et al., 2005), was also measured. Noticeable enhancement in the GSL5 expression was observed in *rss1* followed by *rss2* (Fig. 4G). Taken together, our results indicate that *RSS1* is actively involved in both pre-and post-invasive defense response, as a mutation in this gene leads to elicited accumulation of ROS and papillae formation. Furthermore, rapidly activated cellular defense response without any hypersensitive response to infection by *RS* in Col-0 indicates its *IMPA2*-mediated NHR.

3.5. *RS infection in rss1 affects photosynthetic efficiency and chlorophyll biosynthesis*

Chloroplast biosynthesis plays a major role during plant immunity where mesophyll chloroplasts are the common regulator of photosynthesis (Irieda and Takano, 2021; Serrano et al., 2016). Interestingly, microscopic autofluorescence images and the observations of *RS* challenged *rss1* leaves at 2 dpi displayed a reduced amount and their distribution of photosynthetic pigment. The dynamics of pigments in the mesophyll of infected leaves of Col-0 showed higher chloroplast autofluorescence with unbounded clustering within the cells. On the

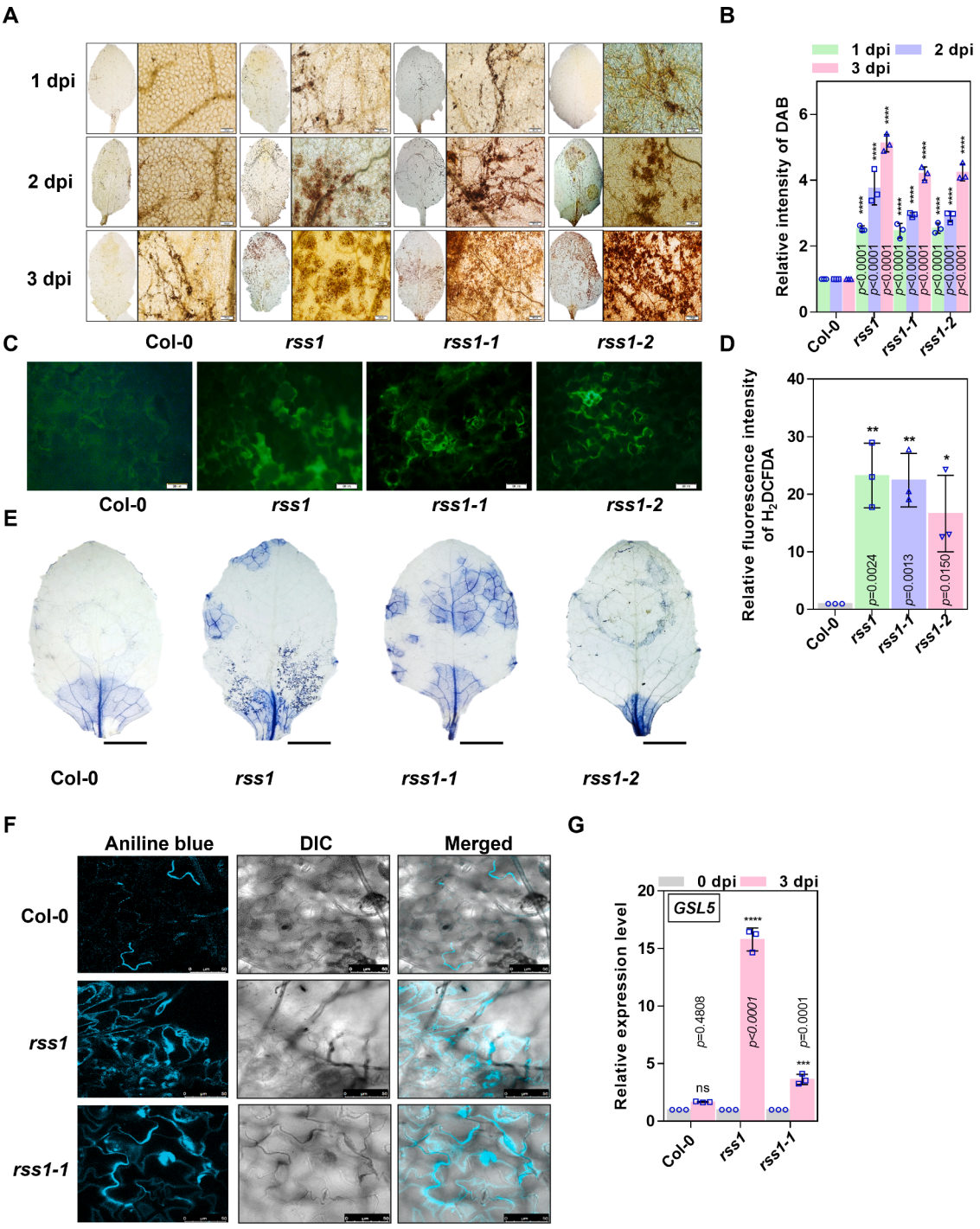

Fig. 4. Mutants exhibited higher ROS accumulation upon challenge with *RS*. (A) Leaves from 24th-day old seedlings of Col-0, *rss1, rss1–1,* and *rss1–2* were infected with *RS* sclerotia and were studied at 1, 2, and 3 dpi with DAB staining for analysis. DAB staining showed a significantly higher accumulation of H_2O_2 (indicated as a brown precipitate) in *rss1, rss1–1*, and *rss1–2* compared to Col-0 with increasing time points. Bar=100 μm. (B) The intensities of DAB-stained leaves of *rss1, rss1–1,* and *rss1–2* were quantified and normalized with the intensity of Col-0 obtained from GIMP. The bar represents the mean (± SD) from three biological replicates (n = 3). Unpaired Student's *t*-test was performed for significance analysis. (C) Also, the infected seedlings were stained using H_2DCFDA (green) at 30 hpi and observed under the Olympus IX71 microscope. Bar=50 μm. (D) Fluorescence intensity was measured in *rss1, rss1–1,* and *rss1–2* and normalized with the intensity of Col-0 obtained from GIMP. The bar represents the mean (± SD) from three biological replicates (n = 3). Unpaired Student's *t*-test was performed for significance analysis. (E) NBT stained Arabidopsis accessions at 3 dpi. Bar=5 mm. (F) Aniline stained autofluorescence photomicrographs of Arabidopsis accessions at 3 dpi representing the attempted sites by *RS*. Bar=50 μm. (G) Quantitative RT-qPCR analysis of the *GSL5*, a callose synthase representing the severity of infection in *rss1* and *rss1–1* at 3 dpi. The bar represents the mean (± SD) from three biological replicates (n = 3). Unpaired Student's *t*-test was performed for significance analysis.

contrary, Col-0 and *rss1* showed indistinctive chloroplast autofluorescence in the mock leaves (Fig. 5A). Since the effect of *RS* infection in *rss1* is seen on its biosynthesis, we quantified chlorophyll (chl) pigments. *RS* infection led to a maximum decrease in the content of chl a (Fig. 5B), chl b (Fig. 5C), and total chl (Fig. 5D) as the time progressed as compared to Col-0. The T-DNA insertion lines also showed a lower amount of chlorophyll pigments; however, the pattern was similar for chl b and total chl but *rss1* showed a drastic reduction in chl a, compared

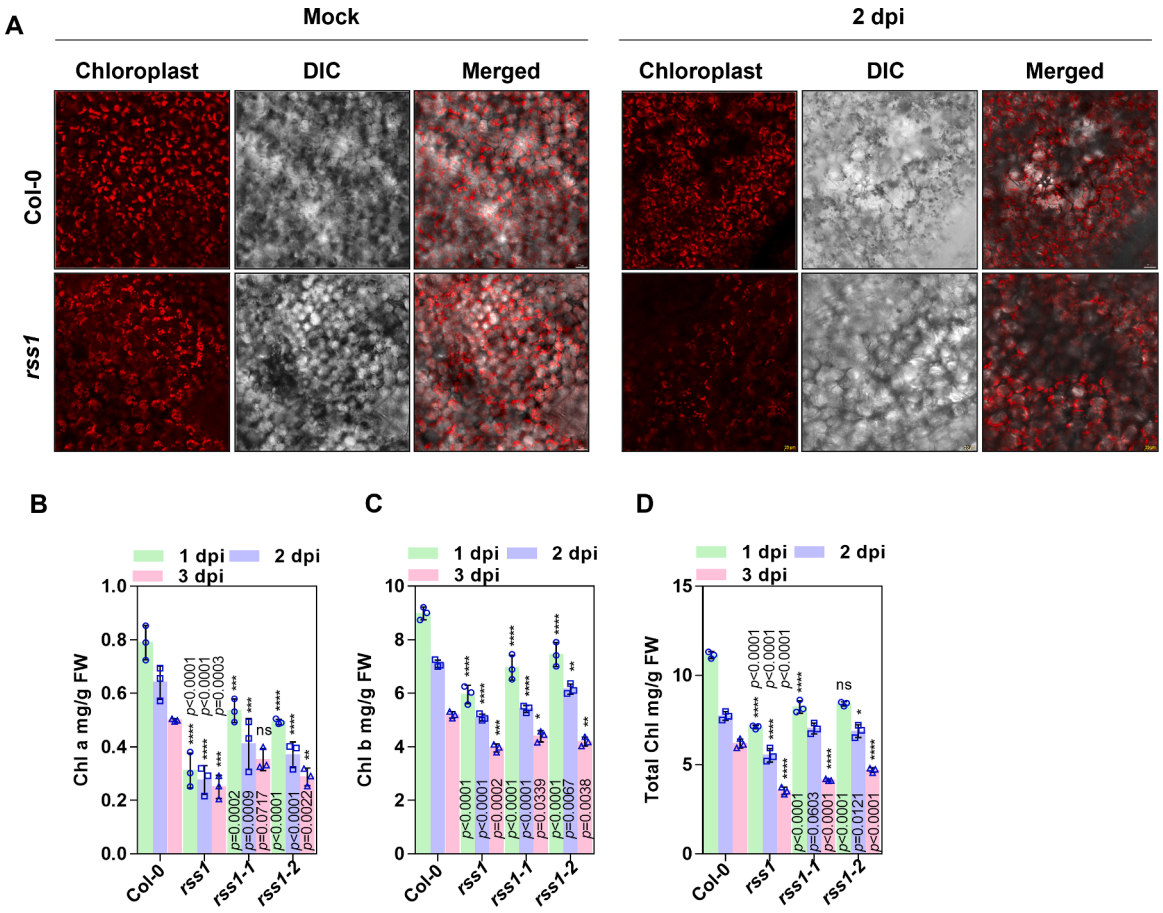

Fig. 5. Evaluation of chlorophyll autofluorescence and quantification of photosynthetic pigments in *RS* challenged leaves of *rss1*. (A) The mesophyll chloroplasts of mock and *RS* inoculated leaves were pictured based on chlorophyll autofluorescence, captured by confocal microscope at the 2 dpi. Bar=20 μm. (B-D) Comparison of chlorophyll pigment (Chl a, Chl b and total) contents from the infected leaves of Col-0 and *rss1, rss1–1, rss1–2* measured at 1, 2, and 3 dpi. The graph represents mean (± SD) which were calculated from nine leaf disks per treatment, with three replicates within an experiment. Similar results were obtained in three independent experiments.

to Col-0. This data indicates that in the absence of *RSS1* the released effector or toxins from *RS* during infection might act on the chloroplastic proteins deleteriously. This might lead to reduced chlorophyll synthesis, consequently directing to impede in photosynthesis and associated defenses resulting from this center.

3.6. Mutation in IMPA2 affects rss1 seedling phenotype with developmental defects

We aimed to assess developmental processes due to mutation in *RSS1* and performed a seed germination assay of Col-0 and *rss1* under similar illumination, temperature, and humidity conditions. The germination rate of the mutant was slower than that of the Col-0 on the 10th day from seed sowing (Fig. S9Ai, ii). The seeds of Col-0 showed a higher germination rate of 52.6% whereas it was 84.4% in the *rss1* (Fig. S9b). The 15th day old Col-0 and *rss1* mutants showed a significant reduction in the root length in *rss1* was seen as compared to the Col-0 (Fig. S9Aiii). The primary root length of Col-0 and mutant were recorded in the 15th-day-old seedlings and found to be 2.38 cm and 0.66 cm respectively (Fig. S9C). Further, the number of lateral roots in Col-0 was more than that of mutant (Fig. S9D).

Additionally, Col-0 and mutant rosette leaves didn't show any morphological difference except that Col-0 rosette leaves have extended petioles and long-oval-shaped leaves (Fig. S9Aiv). The number of rosette leaves on the 10th, 20th, and 30th day were significantly less in *rss1* i.e., around 2, 7, and 14 respectively which was around 4, 15, and 24 leaves in the Col-0 (Fig. S9E). Several fully developed siliques and several seeds produced per siliques also altered in *rss1* (Fig. S9F, G). Although there was little morphological difference in the silique phenotype of Col-0 and *rss1* (Fig. S9Av), the length of silique did not show any significant difference in length (Fig. S9H). Also, the induction of flowering and length of the plant was deferred in *rss1* (Fig. S9Avi,6i).

3.7. RSS1 provides salicylic acid-mediated defense in response to RS-infection

To elucidate the molecular mechanism involved during *RS* pathogenesis, well-characterized subsets of defense-related signaling pathway component reporter genes were inspected in Col-0, *rss1,* and *rss1–1* with an increase in time course by RT-qPCR. We observed significantly induced expression of *PDF1.2a* upon infection that kept on increasing up to 3 dpi in *rss1, rss1–1,* and rice (Fig. 6A). However, Col-0 showed a marginal increase in *PDF1.2a* expression. As a measure of defense to the invading pathogen, Col-0 showed a gradual increase in expression of ~13-fold at 3 dpi of *PR1* (SA response and immunity) and mutants including rice had a decrease in expression concerning time. This may be resulting from compromise in immunity and worked as an antagonistic marker expression (*PDF1.2*) as seen for the jasmonic acid. Surprisingly, the response of *PR1* expression to infection showed a steep increase at 1 dpi in *rss1, rss1–1,* and rice (~18, ~14, and ~15 fold respectively) (Fig. 6B) whereas only 2.5-fold overexpression was seen in Col-0. The spiked enhancement in *PR1* expression in mutants and rice at 1 dpi upon *RS* infection and its downregulation with an increase of *PDF1.2* expression suggests that the necrotrophic phage of the pathogen is

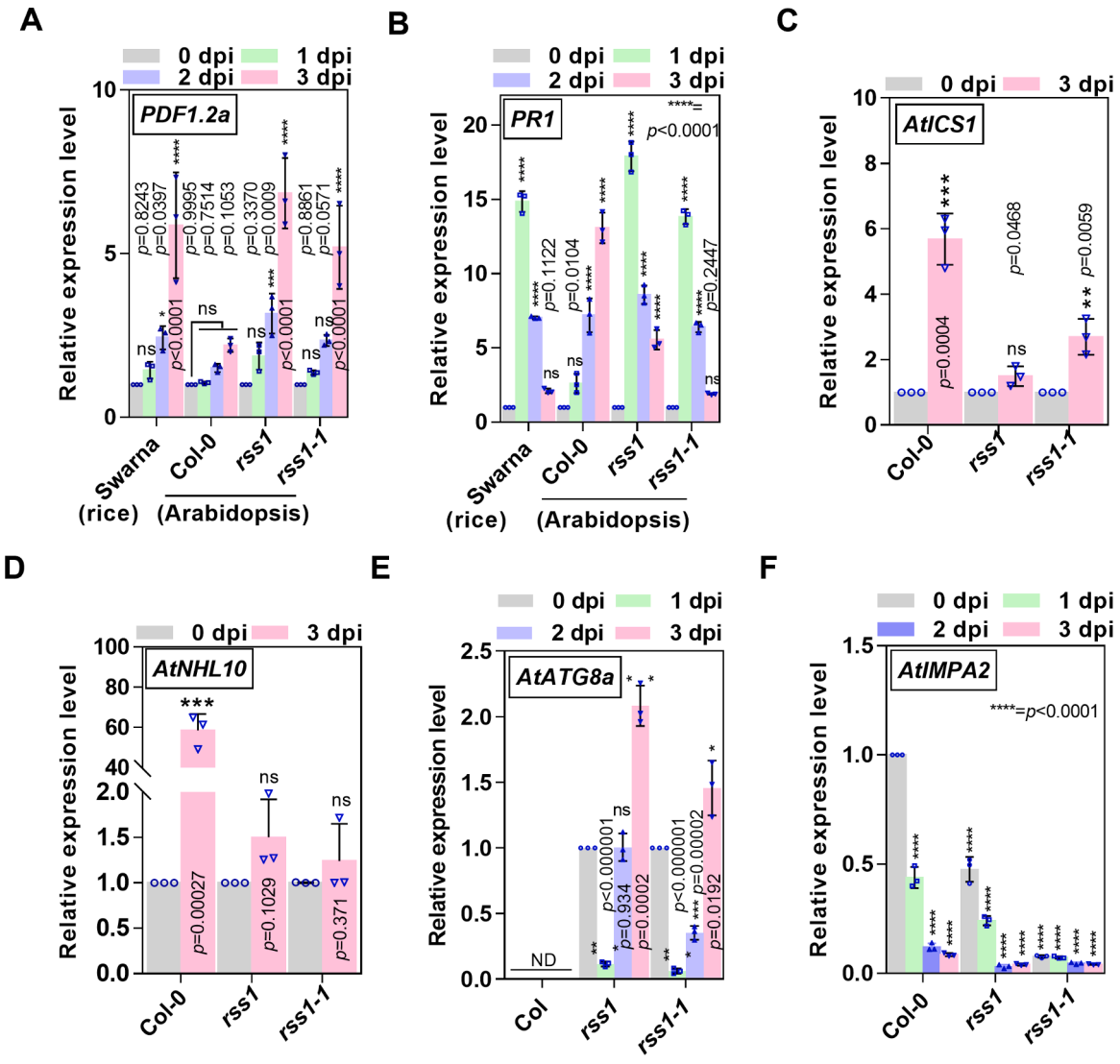

Fig. 6. The expression of defense gene, autophagic markers, and *IMPA2*. Quantification of time-dependent expression of (A) *PDF1.2a*, (B) *PR1*, (C) *ICS1*, (D) *NHL10*, (E) *ATG8a*, and (F) *IMPA2* in the infected leaf samples at 1, 2, and 3 dpi compared with uninfected (0 dpi) leaf samples of Col-0 and respective mutants which were normalized using Arabidopsis *ACTIN2* gene. All the above graphs represent the mean (± SD), with three replicates within an experiment. Similar results were obtained in three independent experiments.

activated upon subduing early defense. Furthermore, enhancement in *PR1* expression correlating to the studied disease resistance phenotype up to 3dpi in Col-0 marks that there is an active SA mediated immunity against *RS* infection. We also investigated the expression pattern of the gene *ICS1* that is required for SA biosynthesis and observed that its expression at 3dpi in Col-0 was ~6 fold whereas, in the *rss1* and *rss1–1*, it was only <2- and <3-fold respectively. This result further confirms the SA mediated active defense in Col-0 against *RS* governed by *IMPA2* (Fig. 6C). To check the elevation in HR to *RS* challenge, the expression pattern of *AtNHL10* was studied and we found that ~60-fold increased expression in Col-0 at 3-dpi but none in *rss1* and *rss1–1* (Fig. 6D) indicating the SA signaling pathway involvement in immunity in Arabidopsis (Zheng et al., 2004).

We reasoned that the infected cells in *rss1* and *rss1–1* might be leading to autophagic cell death and determined the *AtATG8a* expression pattern during the infection. We did not observe any expression of *ATG8* in Col-0 upon infection which also correlates with the infection phenotype where no infection cushions or tissue damage was observed. This suggests that induction of autophagic cell death in Col-0 is not seen, possibly by the active function of *IMPA2* (Fig. 6E). On the contrary, *rss1* and *rss1–1* showed enhanced expression of *ATG8* with an indication that autophagic cell death induced by *RS* signifying successful empowerment of its necrotrophic behavior (Wang et al., 2020). We wanted to investigate if *IMPA2* expression is also regulated by *RS* infection and observed gradual downregulation in its expression in Col-0 signifying its effect on the active participation during immunity. On the other hand, the water control samples of *rss1* showed a decrease in expression which even showed further decreased expression as time progressed and weaker expression in the *rss1–1* (Fig. 6F). We did not observe any expression of *ATG6* and *SEN1* signifying the absence of related pathways for defense or no involvement of them in *RS* infection.

3.8. A homolog of IMPA2 and nuclear RAN1 functions together in triggering immunity

The homology search analysis depicted IMPA1 as the close homolog with P conserved like IMPA2 (Fig. 7A). To access the plausible involvement of *IMPA1*, the screening of a homozygous T-DNA insertion line in *IMPA1* (SALK_082616) was performed. It showed a similar susceptible phenotype that indicates both *IMPA2* and *IMPA1* independently are involved in providing resistance against *RS* (Fig. 7). Although rice ortholog (*Os01g14950*) has conserved proline at 60th position, it is

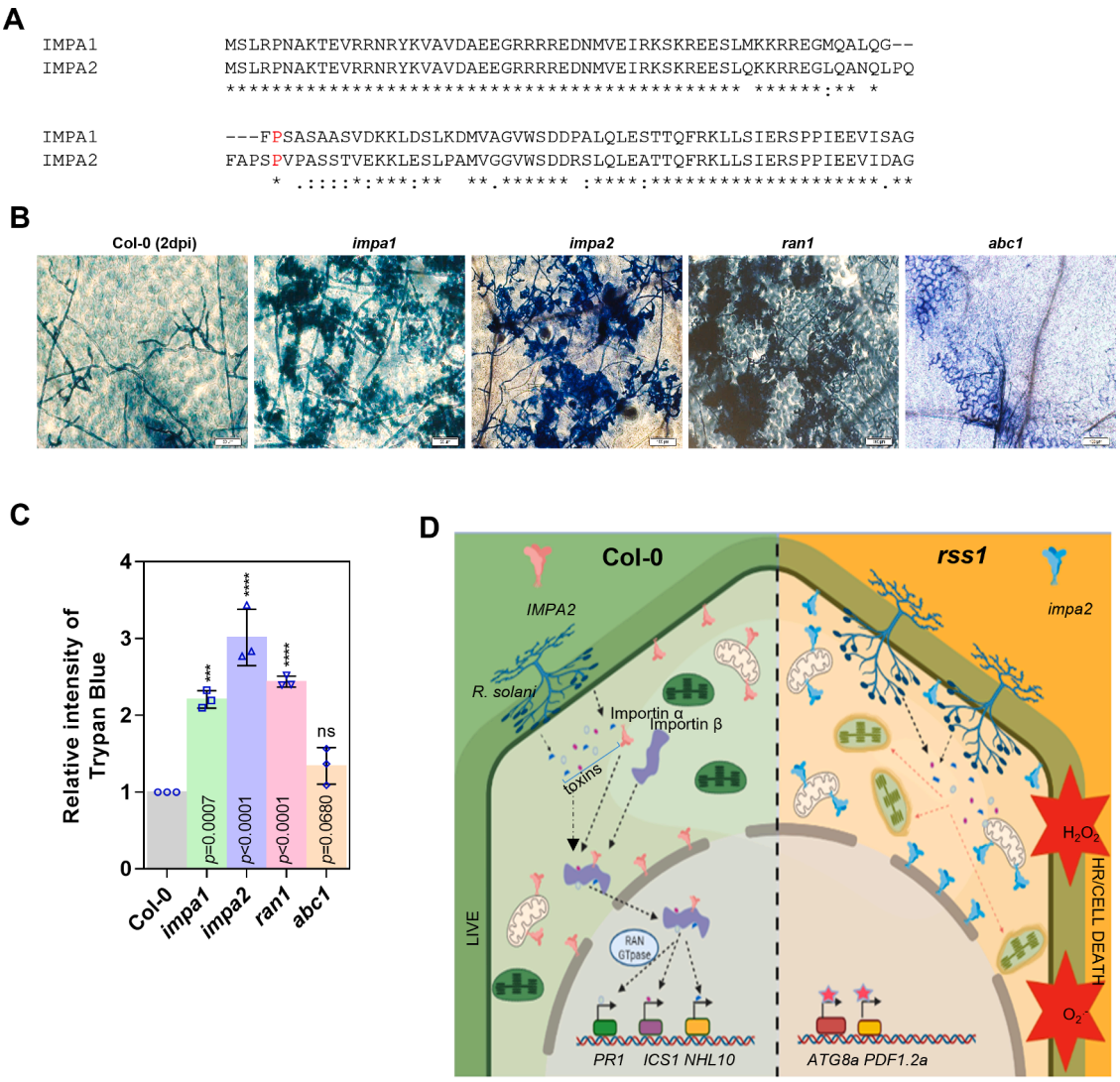

Fig. 7. Disease susceptibility phenotype of *impa1* and *ran1* comparable to *impa2* assessed with Col-0. (A) Clustal W alignment of IMPORTIN ALPHA 1 and 2 depicting the conserved P at 65th position of IMPORTIN ALPHA 2. (B) Detached leaf infection assay of 24th-day old leaves of *impa1, impa2* and *ran1* at 2 dpi showed nearly similar disease severity with infection cushions over the leaf surface stained with trypan blue. (C) *impa1, impa2*, and *ran1* infection phenotypes were also compared to a Salk accession of *abc1* which indicates that the infection severity is independent of T-DNA insertion. (D) Model of *IMPA2*-mediated nonhost resistance in Arabidopsis against *RS*. The toxins from *RS* are detected and bound by *IMPA2* which again bind to importin beta and make a ternary complex that enters the nucleus. Ran GTPase releases the toxin and activates defense responsive genes viz. *PR1, ICS1*, and *NHL10*. However, in *rss1*, toxins of *RS* harm plastids and lead to necrotrophy by evoking HR mediated by *ATG8a* that in turn establish itself to derive nutrition.

working as a host to *RS*, whereas Col-0 with its wild type *IMPA2* is nonhost. Further, to ascertain the functionality of the ternary complex made from the binding of importin α and importin β that transports inside the nucleus and further destabilization of the complex *via* GTP bound RAN protein inside nucleoplasm (Lüdke et al., 2021), we chose to study the involvement of *RAN1*(*At5g20010*). Surprisingly, we found that the knockout mutant of *RAN1* also showed a similar susceptibility response towards infection by *RS*, which however was not seen in the case of another knockout mutant of *ABC1* (*SALK_045739*) (Fig. 7B,C). The subcellular localization of *IMPA2* denotes higher expression in cytosol followed by the nucleus and is lower in the cell wall, plasma membrane, mitochondria, and Golgi but no expression is seen in the plastid (bar.utoronto.ca/cell_efp). The above result suggests that *IMPA2, IMPA1*, and *RAN1* function together and activate immunity against *RS* (Fig. 7D).

Taken together, we mapped the *Rss1* on Ch 4 to 844.6 Kb on its southern arm that is flanked by *JAERI18* and *Ch4_9.18*. NGS data analysis and SNP calling identified two non-synonymous mutations in the mapped region, screening of the T-DNA insertion mutants confirmed that *IMPA2* is the *RSS1* gene. The HR and autophagic cell death upon pathogen invasion in mutants are regulated by *IMPA2*. Although *IMPA2* is downregulated upon infection, the NHR in Col-0 is mediated by the SA biosynthesis pathway at the early hours.

4. Discussion

4.1. *IMPA2 impaired at $^{P}65_{S}$ in Arabidopsis shows breached immunity to RS*

Although there has been no report on the potential rice resistant germplasm, natural nonhost variants that diverged across evolutionary timescale provide resistance by curtailing the early stages of growth in Arabidopsis against *RS* (Parween et al., 2021). Here we have applied forward genetics and identified *IMPA2* (a karyopherin), an NHR gene that provides resistance mediated by SA biosynthetic pathway activation. The identified NHR gene, *At4g16143* encodes an *IMPA2* which is

ubiquitously expressed bearing nuclear localizing signal, NLS. There are 9 paralogs of importin in Arabidopsis with 10 ARM repeat domains whereas six orthologs in rice (Table S7). The distinct functionalities of a specific group of importins in Arabidopsis and rice indicate that the individual importin mediates unique modalities of nuclear import (Quensel et al., 2004). A compromise in the signaling of immunity upon mutation in *IMPA3* has been reported to function upon interaction with mutated *SNC1* (TIR-NBS-LRR-type) (Palma et al., 2005). Arabidopsis *IMPA3* mutation leads to nucleocytoplasmic SNC indicating the requirement of this protein for import of specific signaling components to the nucleus (Zhu et al., 2010). Specific interaction and their import to the nucleus is seen in the case of effectors Nuk6 and Nuk7 but not Nuk12 of *P. infestans* upon silencing of *N. benthamiana IMPORTIN ALPHA 1* and *IMPORTIN ALPHA 2* (Kanneganti et al., 2007). Arabidopsis *IMPORTIN ALPHA 4* has a significant contribution as a requirement in T-complex transport, VirE2 and VirD2 import to nucleus towards the successful transformation by *Agrobacterium* (Bhattacharjee et al., 2008). A wide array of effectors have been reported to localize to nuclei that indicate their sequestration via import or passive diffusion (Caillaud et al., 2012; Deslandes and Rivas, 2011). Hetero trimerization of importin alpha loaded with target protein *via* binding to the armadillo domains with importin beta 1 ferry to the nucleus and with the help of Ran GTP it dissociates and is recycled back to the cytoplasm (Lüdke et al., 2021; Mattaj and Englmeier, 1998; Miyamoto et al., 2016). Our results of specific susceptible disease phenotype in the EMS generated *rss1* with the truncated $^{P}65_{S}$ in the IBB domain which is autoregulatory and the *rss1–1* where no expression of *IMPA2* is seen (Fig 2F). This may indicate the target-specific binding of the protein to the cargo peptides for downstream activation of the defense signaling cascade. In addition to the function of *IMPA2, IMPA1* also has a pivotal role in defending the pathogen (Fig. 7). Also, IMPA2 interacts with RANBP1A (https://genemania.org/) and RANBP1A interacts with RAN1, RAN2, and RAN3 (Haizel et al., 1997). *RAN1* also functions in defense signaling which is confirmed from the knockout phenotype study against RS (Fig. 7). Whether there is any canonical NLS signal with the effector(s) or specific group of putative toxins of *RS* that are secreted during the onset of infection and what are the molecular interacting partners in defining the resistance in Col-0 needs further studies.

4.2. Mutation in RSS1 activates early defense in Arabidopsis in response to RS and negatively regulate chlorophyll biosynthesis

The degree of infection cushion formation and cell death in the mutants was comparable to rice. The rapid accumulation of H_2O_2, $O_2^{\cdot-}$ and deposition of callose at the infection sites are the major hallmark events of cellular defense response in plant cells (Conrath et al., 2001) which play pivotal roles in defense against necrotrophic fungal intruders (Lopez-Cruz et al., 2017; Su'udi et al., 2011). We studied the accumulation of H_2O_2, $O_2^{\cdot-}$ and deposition of callose in NHR to *RS* infection. The results of dramatic difference in the *rss1, rss1–1,* and *rss1–2* as compared to Col-0 suggests that cellular defense is activated in response to infection and entry of the fungal mycelia (Fig. 3). Intriguingly, the cell death did not curtail the further growth of the pathogen and the infection still aggravated suggests that the cell death during HR is a consequence of the cessation of further growth which is found in the compatible *rss1* (Balint-Kurti, 2019). Epidermal chloroplast is the motile organelles that position immune components and fend off pathogen intruders (Irieda and Takano, 2021). The *rss1* was breached with pre-penetration resistance and the mycelia could establish itself inside the epidermis. Possibly, the effectors target to reduce the Chlorophyll *b*iogenesis and the infected leaves showed reduced content of the photosynthetic pigments (Fig. 5). Furthermore, the developmental control of the EMS mutant indicates the possible role of *IMPA2* (Fig. 6).

4.3. SA activates immunity against RS and impa2 shows autophagic cell death

Activation of the signature defense pathway genes in biotic stress is reported to respond to pathogen entry to the tissue (Chan and Zimmerli, 2019). We also aimed to investigate the responses underlying the responses to *RS* infection and found that the *PR1* expression was induced in Col-0 which may be because early defense responses with no establishment of the fungus are provided by SA mediated defense (Fig. 7). However, the mutants showed the opposite trend with a huge increase of *PR1* expression at the onset of infection and thereby a decrease at 3 dpi. The SA biosynthesis marker expression was also elevated in response to *RS* infection confirming the SA mediated defense response in Col-0 at the early hours of immunity. Interestingly, the HR marker gene *NHL10* was found to elevate ~60 fold in Col-0 even at 3 dpi but none at 3 dpi confirming the fact that the cell death in mutants is pathogen-induced and Col-0 showed HR and did not allow the formation of infection cushions. The wheat pathogen, Parastagonospora nodorum, a necrotroph induces programmed cell death by secreting the host-specific toxins to derive nutrition and do not block further invasion (Lorang, 2019). Our results on the induction of the *ATG8* in *rss1* and *rss1–1* but null in the Col-0 correlate with the *RS*-induced autophagic cell death with plausible toxins/effectors as seen in the photomicrographs (Figs. 3, 4, and 7). However, further studies are required/ to confirm the autophagy regulation conferred by *IMPA2*. The downregulation in the expression of the *IMPA2* in *RS* challenged leaves indicates that it positively regulates the immunity against the establishment and subverting the gene expression helps it in establishing the mycelial mass after 3 dpi in the nonhost, Col-0. Furthermore, the minor expression of the gene does not perform any function in activating HR and leads to death from which the fungus derives nutrition. However, which effectors or toxins are involved in infection and what is the path of nuclear programming in immunity in Arabidopsis against *RS* remains to be investigated.

In summary, the Arabidopsis *IMPA2* has a significant contribution towards activating HR against *RS*. The functionality of *IMPA2* plausibly might be in the transport of the cargo effectors that prove vital in immunity against *RS* in plants. This provides evidence on the first clue for the involvement of an NHR gene, *IMPA2* against *RS* infection. This would be possibly helpful for use to genetically engineer elite rice cultivars with improved immunity that is durable, broad-spectrum, and lead a sustainable environment.

Financial support

Supported by the S & T Division, Govt. of Odisha (Grant number 27,552,800,232,014)

Data availability

Data will be available upon request.

Supplementary information

Table S1. Chi-square tests for Mendelian 3:1 segregation of the Col-0 (resistant) to *rss1* (susceptible).

Table S2. Fine mapping of *RSS1* using individual $F_{2:3}$ susceptible samples on Chromosome 4.

Table S3. List of putative *RSS1* genes identified from the NGM analysis pipeline upon alignment onto Col-0 reference sequence.

Table S4. Details of the SALK T-DNA insertion lines used for confirmation of the mutation.

Table S5. List of SSLP primers used for qPCR.

Table S6. List of primers used for RT-qPCR.

Table S7. Percentage of similarity index of IMPA2 with 9 paralogs in Arabidopsis and six orthologs in rice.

Fig. S1. Phenotype and screening of EMS mutated M_3 plants.

Fig. S2. Genotype confirmation of F_1 and phenotype screening of F_2 plants from 0.3% EMS mutated plants.

Fig. S3. Micrographs of Calcofluor White stained surface mycelia of *RS*.

Fig. S4. Chromosomal mapping and polymorphism showed by SSLP markers in Chromosome 1.

Fig. S5. Chromosomal mapping and polymorphism showed by SSLP markers in Chromosome 2.

Fig. S6. Chromosomal mapping and polymorphism showed by SSLP markers in Chromosome 3.

Fig. S7. Chromosomal mapping and polymorphism showed by SSLP markers in Chromosome 4.

Fig. S8. Chromosomal mapping and polymorphism showed by SSLP markers in Chromosome 5.

Fig. S9. Comparison of the phenotypic variations between wild type and EMS generated mutant explained impaired development in *rss1*.

CRediT authorship contribution statement

Daraksha Parween: Visualization, Investigation, Formal analysis, Writing – original draft. **Binod Bihari Sahu:** Conceptualization, Supervision, Formal analysis, Writing – original draft.

Declaration of Competing Interest

The authors declare the following financial interests/personal relationships which may be considered as potential competing interests: Daraksha Parween reports financial support was provided by Science and Technology department, Government of Odisha.Binod Bihari Sahu reports financial support was provided by Science and Technology Department, Government of Odisha

Acknowledgments

We thank Arup K. Mukherjee, NRRI, Cuttack for providing the virulent *RS* strain. We thank the Director, National Institute of Technology, Rourkela, Central instrumentation facility of the department, and Sushant Kumar Pradhan in assisting the confocal imaging. We also thank Dr. Eram Sultan and Debasish Pati for the NGM analysis and artworks. The authors thank Dr. Sujit K. Bhutia and Dr. Rohan Dhiman for kindly reviewing and editing the manuscript and for their valuable comments.

Supplementary materials

Supplementary material associated with this article can be found, in the online version, at doi:10.1016/j.crmicr.2022.100109.

References

Aist, J., 1976. Papillae and related wound plugs of plant cells. Annu. Rev. Phytopathol. 14, 145–163.

Alexandratos, N., and Bruinsma, J. 2012. World agriculture towards 2030/2050: the 2012 revision.

Alonso, J.M., Stepanova, A.N., Solano, R., Wisman, E., Ferrari, S., Ausubel, F.M., Ecker, J. R, 2003. Five components of the ethylene-response pathway identified in a screen for weak ethylene-insensitive mutants in Arabidopsis. Proc. Natl. Acad. Sci. U. S. A. 100, 2992–2997.

Austin, R.S., Vidaurre, D., Stamatiou, G., Breit, R., Provart, N.J., Bonetta, D., Zhang, J., Fung, P., Gong, Y., Wang, P.W, 2011. Next-generation mapping of Arabidopsis genes. Plant J. 67, 715–725.

Balint-Kurti, P., 2019. The plant hypersensitive response: concepts, control and consequences. Mol. Plant Pathol. 20, 1163–1178.

Basu, A., Chowdhury, S., Ray Chaudhuri, T., Kundu, S., 2016. Differential behaviour of sheath blight pathogen *Rhizoctonia solani* in tolerant and susceptible rice varieties before and during infection. Plant Pathol. 65, 1333–1346.

Bhattacharjee, S., Lee, L.Y., Oltmanns, H., Cao, H., Cuperus, J., Gelvin, S.B, 2008. IMPa-4, an Arabidopsis importin α isoform, is preferentially involved in Agrobacterium-mediated plant transformation. Plant Cell 20, 2661–2680.

Bolwell, G.P., Daudi, A., 2009. Reactive oxygen species in plant–pathogen interactions. Reactive Oxygen Species in Plant Signaling. Springer, pp. 113–133.

Caillaud, M.C., Piquerez, S.J., Fabro, G., Steinbrenner, J., Ishaque, N., Beynon, J., Jones, J.D, 2012. Subcellular localization of the Hpa RxLR effector repertoire identifies a tonoplast-associated protein HaRxL17 that confers enhanced plant susceptibility. Plant J. 69, 252–265.

Chan, C., Zimmerli, L., 2019. The histone demethylase IBM1 positively regulates Arabidopsis immunity by control of defense gene expression. Front. Plant Sci. 10, 1587.

Conrath, U., Thulke, O., Katz, V., Schwindling, S., Kohler, A., 2001. Priming as a mechanism in induced systemic resistance of plants. Eur. J. Plant Pathol. 107, 113–119.

Denby, K.J., Kumar, P., Kliebenstein, D.J, 2004. Identification of *Botrytis cinerea* susceptibility loci in *Arabidopsis thaliana*. Plant J. 38, 473–486.

Deslandes, L., Rivas, S., 2011. The plant cell nucleus: a true arena for the fight between plants and pathogens. Plant Signal Behav. 6, 42–48.

Dongus, J.A., Bhandari, D.D., Patel, M., Archer, L., Dijkgraaf, L., Deslandes, L., Shah, J., Parker, J.E, 2020. The Arabidopsis PAD4 lipase-like domain is sufficient for resistance to green peach aphid. Mol. Plant Microbe Interact. 33, 328–335.

Ellinger, D., Voigt, C.A, 2014. Callose biosynthesis in Arabidopsis with a focus on pathogen response: what we have learned within the last decade. Ann. Bot. 114, 1349–1358.

Enns, L.C., Kanaoka, M.M., Torii, K.U., Comai, L., Okada, K., Cleland, R.E, 2005. Two callose synthases, GSL1 and GSL5, play an essential and redundant role in plant and pollen development and in fertility. Plant Mol. Biol. 58, 333–349.

Ferrari, S., Plotnikova, J.M., De Lorenzo, G., Ausubel, F.M, 2003. Arabidopsis local resistance to *Botrytis cinerea* involves salicylic acid and camalexin and requires *EDS4* and *PAD2*, but not *SID2, EDS5* or *PAD4*. Plant J. 35, 193–205.

Fonseca, J.P., Mysore, K.S, 2019. Genes involved in nonhost disease resistance as a key to engineer durable resistance in crops. Plant Sci. J. 279, 108–116.

Fryer, M.J., Oxborough, K., Mullineaux, P.M., Baker, N.R, 2002. Imaging of photo-oxidative stress responses in leaves. J. Exp. Bot. 53, 1249–1254.

Gill, U.S., Lee, S., Mysore, K.S, 2015. Host versus nonhost resistance: distinct wars with similar arsenals. Phytopathology 105, 580–587.

Haizel, T., Merkle, T., Pay, A., Fejes, E., Nagy, F., 1997. Characterization of proteins that interact with the GTP-bound form of the regulatory GTPase Ran in Arabidopsis. Plant J. 11, 93–103.

Hematy, K., Lim, M., Cherk, C., Pislewska-Bednarek, M., Sanchez-Rodriguez, C., Stein, M., Fuchs, R., Klapprodt, C., Lipka, V., Molina, A., 2020. Moonlighting function of phytochelatin synthase1 in extracellular defense against fungal pathogens. Plant Physiol. 182, 1920–1932.

Irieda, H., Takano, Y., 2021. Epidermal chloroplasts are defense-related motile organelles equipped with plant immune components. Nat. Commun. 12, 1–19.

Jamra, G., Agarwal, A., Singh, N., Sanyal, S.K., Kumar, A., Pandey, G.K, 2021. Ectopic expression of finger millet calmodulin confers drought and salinity tolerance in *Arabidopsis thaliana*. Plant Cell Rep. 40, 2205–2223.

Kambakam, S., Ngaki, M.N., Sahu, B.B., Kandel, D.R., Singh, P., Sumit, R., Swaminathan, S., Muliyar-Krishna, R., Bhattacharyya, M.K, 2021. Arabidopsis non-host resistance *PSS30* gene enhances broad-spectrum disease resistance in the soybean cultivar Williams 82. Plant J. 107, 1432–1446.

Kang, L., Li, J., Zhao, T., Xiao, F., Tang, X., Thilmony, R., He, S., Zhou, J.M., 2003. Interplay of the Arabidopsis nonhost resistance gene *NHO1* with bacterial virulence. Proc. Natl. Acad. Sci. U. S. A. 100, 3519–3524.

Kanneganti, T.D., Bai, X., Tsai, C.W., Win, J., Meulia, T., Goodin, M., Kamoun, S., Hogenhout, S.A, 2007. A functional genetic assay for nuclear trafficking in plants. Plant J. 50, 149–158.

Khare, D., Choi, H., Huh, S.U., Bassin, B., Kim, J., Martinoia, E., Sohn, K.H., Paek, K.H., Lee, Y., 2017. Arabidopsis *ABCG34* contributes to defense against necrotrophic pathogens by mediating the secretion of camalexin. Proc. Natl. Acad. Sci. U. S. A. 114, E5712–E5720.

Kiraly, L., 2002. mlo5, a resistance gene effective against a biotrophic pathogen (Blumeria graminis fsp. hordei) confers enhanced susceptibility of barley to the necrotrophic fungus Bipolaris sorokiniana (teleomorph: cochliobolus sativus). Acta Biol. Szeged. 46, 135–136.

Lapin, D., Bhandari, D.D., Parker, J.E, 2020. Origins and immunity networking functions of EDS1 family proteins. Annu. Rev. Phytopathol. 58, 253–276.

Letunic, I., Khedkar, S., Bork, P., 2020. SMART: recent updates, new developments and status in 2020. Nucleic Acids Res. 49, D458–D460. https://doi.org/10.1093/nar/gkaa937.

Li, D., Li, S., Wei, S., Sun, W., 2021. Strategies to manage rice sheath blight: lessons from interactions between Rice and Rhizoctonia solani. Rice 14, 1–15.

Lipka, V., Dittgen, J., Bednarek, P., Bhat, R., Wiermer, M., Stein, M., Landtag, J., Brandt, W., Rosahl, S., and Scheel, D. 2005. Pre-and postinvasion defenses both contribute to nonhost resistance in Arabidopsis. Science 310:1180–1183.

Lopez-Cruz, J., Oscar, C.S., Emma, F.C., Pilar, G.A., Carmen, G.B, 2017. Absence of Cu–Zn superoxide dismutase BCSOD1 reduces *Botrytis cinerea* virulence in Arabidopsis and tomato plants, revealing interplay among reactive oxygen species, callose and signalling pathways. Mol. Plant Pathol. 18, 16–31.

Lorang, J., 2019. Necrotrophic exploitation and subversion of plant defense: a lifestyle or just a phase, and implications in breeding resistance. Phytopathology 109, 332–346.

Lu, M., Tang, X., Zhou, J.M., 2001. Arabidopsis *NHO1* is required for general resistance against Pseudomonas bacteria. Plant Cell 13, 437–447.

Lüdke, D., Roth, C., Kamrad, S.A., Messerschmidt, J., Hartken, D., Appel, J., Hörnich, B. F., Yan, Q., Kusch, S., Klenke, M., 2021. Functional requirement of the Arabidopsis importin-α nuclear transport receptor family in autoimmunity mediated by the NLR protein SNC1. Plant J. 105, 994–1009.

Lukowitz, W., Gillmor, C.S., Scheible, W.R, 2000. Positional cloning in Arabidopsis. Why it feels good to have a genome initiative working for you. Plant Physiol. 123, 795–806.

Maeda, K., Houjyou, Y., Komatsu, T., Hori, H., Kodaira, T., Ishikawa, A., 2009. AGB1 and PMR5 contribute to PEN2-mediated preinvasion resistance to *Magnaporthe oryzae* in *Arabidopsis thaliana*. Mol. Plant Microbe Interact. 22, 1331–1340.

Mattaj, I.W., Englmeier, L., 1998. Nucleocytoplasmic transport: the soluble phase. Annu. Rev. Biochem. 67, 265–306. https://doi.org/10.1146/annurev.biochem.67.1.265.

Micali, C., Gollner, K., Humphry, M., Consonni, C., and Panstruga, R. 2008. The powdery mildew disease of Arabidopsis: a paradigm for the interaction between plants and biotrophic fungi. The Arabidopsis Book/American Society of Plant Biologists 6.

Mishra, D., Rajput, R.S., Zaidi, N.W., Singh, H., 2020. Sheath blight and drought stress management in rice (*Oryza sativa*) through Trichoderma spp. Indian Phytopathol. 73, 71–77.

Miyamoto, Y., Yamada, K., Yoneda, Y, 2016. Importin α: a key molecule in nuclear transport and non-transport functions. J. Biol. Chem. 160, 69–75. https://doi.org/10.1093/jb/mvw036.

Molla, K.A., Karmakar, S., Molla, J., Bajaj, P., Varshney, R.K., Datta, S.K., Datta, K., 2020. Understanding sheath blight resistance in rice: the road behind and the road ahead. Plant Biotechnol. J. 18, 895–915.

Mysore, K.S., Ryu, C.M., 2004. Nonhost resistance: how much do we know? Trends Plant Sci. 9, 97–104.

Ngou, B.P.M., Jones, J.D., Ding, P., 2021. Plant immune networks. Trends Plant Sci. https://doi.org/10.1016/j.tplants.2021.08.012.

Palma, K., Zhang, Y., Li, X., 2005. An importin α homolog, MOS6, plays an important role in plant innate immunity. Curr. Biol. 15, 1129–1135.

Park, J.Y., Jin, J., Lee, Y.W., Kang, S., Lee, Y.H, 2009. Rice blast fungus (*Magnaporthe oryzae*) infects Arabidopsis via a mechanism distinct from that required for the infection of rice. Plant Physiol. 149, 474–486.

Parween, D., Sultan, E., Dalei, K., Sahu, B., 2021. Arabidopsis nonhost resistance gene *PENETRATION 2* is involved in disruption of cushion formation by *Rhizoctonia solani* during early infection process. Aust. Plant. Pathol. 50, 281–292.

Pfaffl, M.W., 2001. A new mathematical model for relative quantification in real-time RT–PCR. Nucleic Acids Res. 29, e45. -e45.

Qu, L.J., and Qin, G. (2014). Generation and identification of Arabidopsis EMS mutants. In Arabidopsis Protocols, Springer: pp. 225–239.

Quensel, C., Friedrich, B., Sommer, T., Hartmann, E., Kohler, M., 2004. *In vivo* analysis of importin α proteins reveals cellular proliferation inhibition and substrate specificity. Mol. Cell. Biol. 24, 10246–10255.

Sahu, B.B., Sumit, R., Srivastava, S.K., Bhattacharyya, M.K, 2012. Sequence based polymorphic (SBP) marker technology for targeted genomic regions: its application in generating a molecular map of the *Arabidopsis thaliana* genome. BMC Genom. 13, 1–10.

Scalschi, L., Llorens, E., Camañes, G., Pastor, V., Fernández Crespo, E., Flors, V., García Agustín, P., and Vicedo, B. 2015. Quantification of callose deposition in plant leaves. 510.21769/BioProtoc.1610.

Schneider, C.A., Rasband, W.S., Eliceiri, K.W, 2012. NIH Image to ImageJ: 25 years of image analysis. Nat. Methods 9, 671–675.

Serrano, I., Audran, C., Rivas, S., 2016. Chloroplasts at work during plant innate immunity. J. Exp. Bot. 67, 3845–3854.

Solano, B.L.M.M.A., 2002. R. Constitutive expression of ETHYLENE-RESPONSE-FACTOR1 in Arabidopsis confers resistance to several necrotrophic fungi. Plant J. 29, 23–32.

Stein, M., Dittgen, J., Sanchez-Rodriguez, C., Hou, B.-.H., Molina, A., Schulze-Lefert, P., Lipka, V., Somerville, S., 2006. Arabidopsis PEN3/PDR8, an ATP binding cassette transporter, contributes to nonhost resistance to inappropriate pathogens that enter by direct penetration. Plant Cell 18, 731–746.

Stone, B., and Clarke, A. 1992. Chemistry and biology of (1-3)-β-Glucans La Trobe university press. Bundoora, Australia:517.

Su'udi, M., Kim, M.G., Park, S.R., Hwang, D.J., Bae, S.C., Ahn, I.P, 2011. Arabidopsis cell death in compatible and incompatible interactions with *Alternaria brassicicola*. Mol. Cells 31, 593–601.

Sumit, R., Sahu, B.B., Xu, M., Sandhu, D., Bhattacharyya, M.K, 2012. Arabidopsis nonhost resistance gene *PSS1* confers immunity against an oomycete and a fungal pathogen but not a bacterial pathogen that cause diseases in soybean. BMC Plant Biol. 12, 1–15.

Thomma, B.P., Eggermont, K., Penninckx, I.A., Mauch-Mani, B., Vogelsang, R., Cammue, B.P., Broekaert, W.F, 1998. Separate jasmonate-dependent and salicylate-dependent defense-response pathways in Arabidopsis are essential for resistance to distinct microbial pathogens. Proc. Natl. Acad. Sci. U. S. A. 95, 15107–15111.

Wang, B., Sumit, R., Sahu, B.B., Ngaki, M.N., Srivastava, S.K., Yang, Y., Swaminathan, S., Bhattacharyya, M.K, 2018. Arabidopsis novel glycine-rich plasma membrane *PSS1* protein enhances disease resistance in transgenic soybean plants. Plant Physiol. 176, 865–878.

Wang, P., Nolan, T.M., Yin, Y., Bassham, D.C, 2020. Identification of transcription factors that regulate ATG8 expression and autophagy in Arabidopsis. Autophagy 16, 123–139.

Yamaura, S., Yamauchi, Y., Makihara, M., Yamashino, T., Ishikawa, A., 2020. CCA1 and LHY contribute to nonhost resistance to *Pyricularia oryzae* (syn. *Magnaporthe oryzae*) in *Arabidopsis thaliana*. Biosci. Biotechnol. Biochem. 84, 76–84.

Yellareddygari, S., Reddy, M., Kloepper, J., Lawrence, K., Fadamiro, H., 2014. Rice sheath blight: a review of disease and pathogen management approaches. J. Plant Pathol. Microbiol. 5, 1.

Zeng, L., Zhou, J., Li, B., Xing, D, 2015. A high-sensitivity optical device for the early monitoring of plant pathogen attack via the *in vivo* detection of ROS bursts. Front. Plant Sci. 6, 96.

Zheng, M.S., Takahashi, H., Miyazaki, A., Hamamoto, H., Shah, J., Yamaguchi, I., Kusano, T., 2004. Up-regulation of Arabidopsis thaliana NHL10 in the hypersensitive response to cucumber mosaic virus infection and in senescing leaves is controlled by signalling pathways that differ in salicylate involvement. Planta 218, 740–750.

Zhu, Y., Qian, W., Hua, J., 2010. Temperature modulates plant defense responses through NB-LRR proteins. PLoS Pathog. 6 e1000844.